Magnetization reversal in exchange-biased Ni/NiO layered structures

J. Ben Youssef, V. Castel, K. Garello, N. Gargam, S. Pogossian, D. Spenato, and D. T. Dekadjevi*
Laboratoire de Magnetisme de Bretagne, Department of Physics, CNRS-UBO, 29285 Brest Cedex 3, France

A. Suvorova
Centre for Microscopy and Microanalysis, University of Western Australia, Crawley, Western Australia 6009, Australia

T. R. Charlton, R. M. Dalgliesh, and S. Langridge
ISIS, Rutherford Appleton Laboratory, Chilton, Oxon OX11 0QX, United Kingdom
(Received 10 April 2007; published 3 October 2007)

The dependence of the asymmetric magnetization reversal, exchange field, and coercive field on the NiO microstructure and thickness is studied in polycrystalline Ni/NiO. Probing structural properties in real and reciprocal space, we show that the modification of the NiO growth conditions results in nonstoichiometric NiO. Exchange and coercive fields are strongly enhanced in nonstoichiometric Ni/NiO bilayers. Probing exchange properties in trilayers, we show that the coercive and exchange field enhancements are of different origins but depend on the NiO domain state. Modifying the internal part of the antiferromagnet allows a control of the exchange properties. Studying the Ni magnetization reversal, we reveal the contribution of nonuniform reversal modes and coherent rotation as a function of the angle between the applied field and the Ni easy axis. We observe two distinct critical angles revealing the significant role of nonuniform magnetization reversal in the asymmetry and its angular dependence.

DOI: 10.1103/PhysRevB.76.134401 PACS number(s): 75.60.Jk, 75.70.Cn, 75.50.Ee

I. INTRODUCTION

Uniaxial anisotropic properties in magnetism open a world of hysteretic behavior. Over 50 years ago, a new kind of anisotropy named unidirectional (or exchange) anisotropy was discovered[1,2] and has now been thoroughly studied to provide a fundamental understanding of magnetization reversal and for applications such as read heads.[3,4] This exchange anisotropy is observed in ferromagnetic (F)/antiferromagnetic (AF) bilayers and is revealed by the hysteresis loop shift along the field axis (H_e) and the coercive field (H_c) enhancement. Experimental observations and theoretical predictions have shown that domain wall (DW) formation in the ferromagnet (F) and/or in the antiferromagnet (AF) should be considered in the reversal mechanism in order to obtain a reasonable value for H_e.[5] Mauri *et al.* suggested the presence of a parallel DW at the interface[6] and later demonstrated experimentally.[7] H_e would then depend on the energy stored in this wall. Defects within this DW are predicted to enhance the H_c.[8] Instead of a parallel DW proposed in those models, Malozemoff[9] followed by Nowak *et al.*[10] predicted that nonuniform magnetization reversal, via the creation of a multidomain structure in the AF, was a driving mechanism of exchange anisotropy. In these models, interfacial or AF bulk defects lead to a random field that breaks the AF layer into domains. H_e originates from the interfacial staggered spins, i.e., the nonreversible part of interfacial spins. The H_c enhancement originates from the reversible process driven by the AF uniaxial anisotropy that procures additional critical fields to hinder the DW motion in the F.[11,12]

Previous experimental studies probed the H_c dependence on the F thickness and its relation with the magnetization reversal process.[13–17] In these approaches, the AF anisotropy was not varied and its relation to H_c was assumed. Probing the AF uniaxial anisotropy and the ability of changing its value experimentally present the major difficulties in further studying the role of the AF. Furthermore, the effect of the AF anisotropy on the magnetization reversal could be attributed to interfacial coupling effects.

Beyond the H_c enhancement, the presence of domains in the magnetization reversal is associated with the unusual properties of exchange-bias systems. Among them, the asymmetric reversal of magnetization has recently received particular attention. This phenomenon is experimentally observed by techniques sensitive not only to the magnitude of the magnetization but also to its vectorial character. Polarized neutron reflectivity,[18] domain imaging,[19] anisotropic magnetoresistance,[20] vectorial Kerr magnetometry,[21–23] and vectorial susceptibility[24] have shown that magnetization reversal may be different on each side of the hysteresis loop and this asymmetry will depend on the angle between the applied field and the F easy axis. The contributions of coherent rotation and domain nucleation to the asymmetry and its angular dependence are outlined but their respective role is still unclear. Recent studies have shown that features of the angular dependence of the asymmetry can be reproduced by coherent rotation reversal.[23,25] These results support the nonrelevance of the nonuniform magnetization reversal, i.e., DW formation, to the asymmetry and its angular dependence. However, Beckmann *et al.* have predicted the relevance of domains using numerical simulations based on the domain state model.[26] In a recent paper, we have shown experimental evidence for the domain contribution to the asymmetric reversal.[27]

In this work, we present a systematic study of the dependence of the most characteristic exchange-bias phenomena on the AF structural and magnetic ordering for Ni/NiO structures. These phenomena include H_e, H_c, the AF critical

 ©2007 The American Physical Society

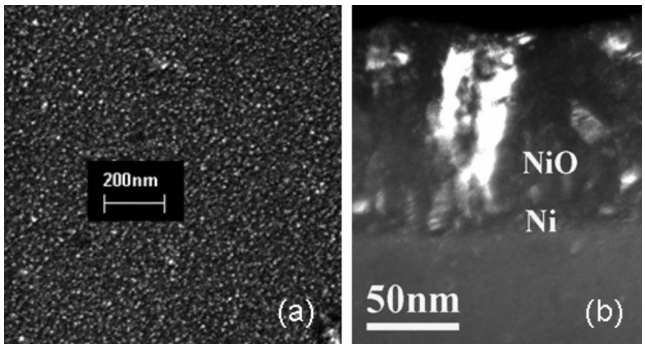

FIG. 1. (a) SEM image of typical surface morphology of a NiO film. (b) Dark-field image of Ni/NiO stack ($g=111$).

thickness, and the asymmetry of the reversal. We modified the NiO magnetic properties through changes in its structural ordering to understand the magnetization reversal mechanism. The structural study of [glass/Ni/NiO] bilayers in real and reciprocal space is first presented. Following this, the unidirectional and coercive field evolution as a function of the NiO disorder and thickness are probed to determine the magnetization reversal properties. In this part of the paper, trilayers containing Ni and NiO are studied to probe the presence of parallel DWs and to examine the relation between H_c and H_e. Finally, the angular dependence of the magnetization reversal is probed as a function of the NiO properties to understand the effect of the F/AF exchange coupling on axial and unidirectional properties.

Structures were grown on glass substrates by rf sputtering under a 300 Oe magnetic field and with a base pressure of 10^{-7} mbar. The NiO layers were obtained from the sputtering of a Ni_1O_1 target. They were grown at different argon gas pressures (P) to modify the structural ordering. In this paper, NiO_P corresponds to a NiO layer grown at the argon base pressure equal to P. Compositional and structural characterizations were performed using field emission scanning electron microscopy (FESEM), transmission electron microscopy (TEM), energy dispersive x-ray spectroscopy (EDS), x-ray reflectometry (XRR), and x-ray diffraction (XRD) techniques. Magnetic measurements were performed at room temperature using a vectorial vibrating sample magnetometer (VSM) and polarized neutron reflectometry (PNR).

II. STRUCTURAL PROPERTIES

We present real space imaging to assess the morphology and crystallographic properties of the bilayers. The morphology was studied using FESEM imaging. Charging of the layers makes it difficult to obtain surface morphology information from conventional, high vacuum SEM. To alleviate this problem, we have used the in-lens secondary electron detector of a Zeiss Supra 55VPSEM, operating at low voltage. As revealed in Fig. 1(a), the surface morphology of a NiO layer clearly displays a grain structure and suggests that the layer is of a crystalline nature. Changing in the growth conditions results in NiO surfaces which maintain the grain structure. Figure 2(a) shows electron diffraction pattern acquired using TEM in the cross-sectional projection. It indicates the polycrystalline nature of both layers. It should be noted that the NiO polycrystalline nature shown by TEM is confirmed by a 25° wide rocking curve on the (111) x-ray peak, for each value of pressure. The comparison of the experimental and theoretical relative intensity of the (111) and (200) Bragg peaks indicates a slight [111] texture. Figure 1(b), obtained on [Ni(53 Å)/NiO_4(700 Å)], shows NiO grains with a rectangular shape, having a width of 190±40 Å and a height of 400 Å. The height was not modified by the growth conditions and the width obtained by TEM was in agreement with FESEM analysis. The Ni grains also had a rectangular shape with a height equal to the thickness and a 40 Å width. Changes in growth condition during the NiO layer growth did not affect the underlying Ni structure.

The chemical information was visualized by generating energy filtered TEM (EFTEM) images of constituent elements. Ni elemental maps, O elemental maps, and energy selected images demonstrate continuous coverage within the NiO films and a well defined Ni layer.[27] The reliability of the EFTEM information depends on the spatial resolution of this technique which in these experiments is ~20 Å. Consequently, short range strain fields caused by defects were undetectable. However, diffraction techniques provide information about defects as they lead to a nonuniform strain.[28] XRD measurements from Bragg planes parallel to the surface were

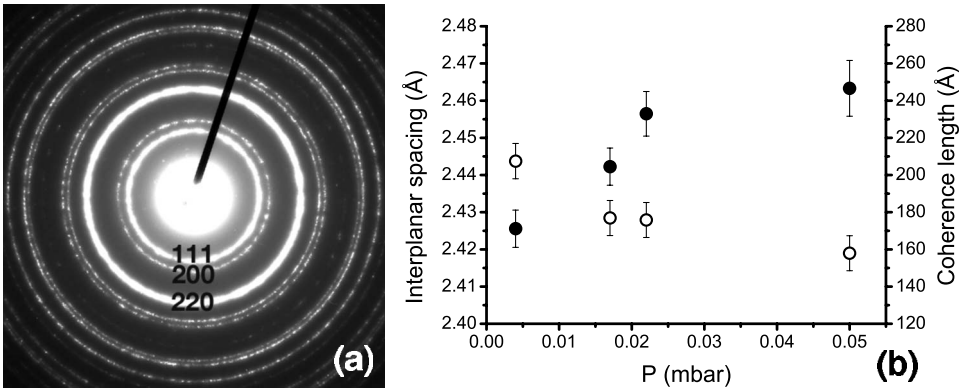

FIG. 2. (a) Selected area electron diffraction pattern from a NiO film. (b) Interplanar spacing (○) and coherence length (●) as a function of P in [Ni(53 Å)/NiO_P(700 Å)].

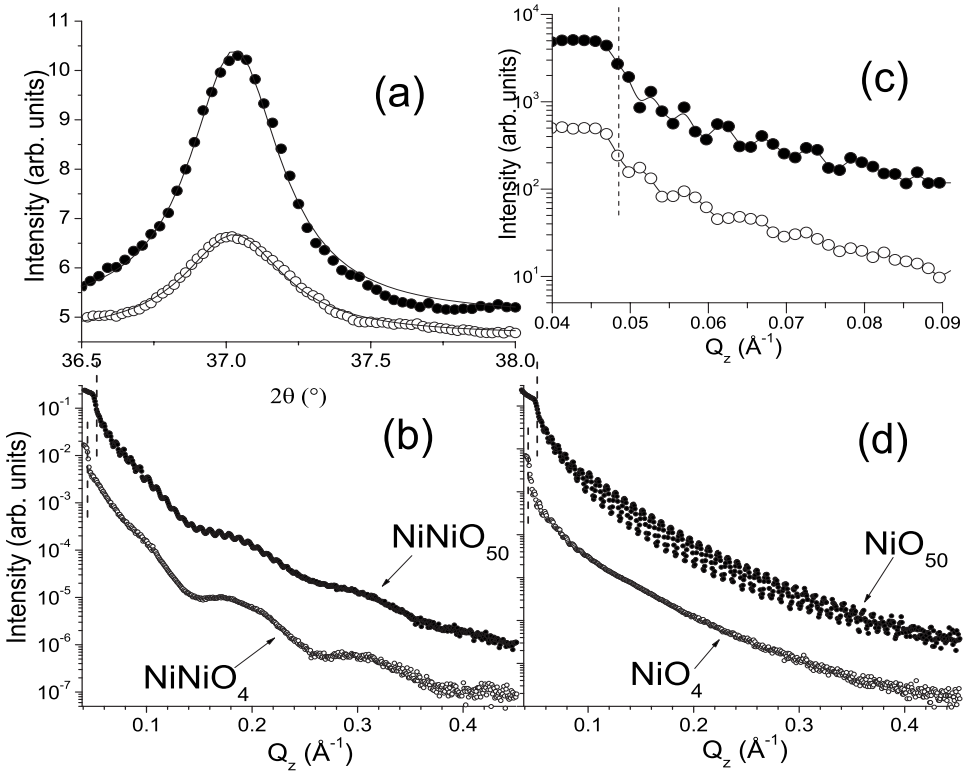

FIG. 3. (a) High angle x-ray diffraction scans for Ni/NiO_{25}(700 Å) (●) and Ni/NiO_{25}(220 Å) (○). (b) X-ray reflectivity scans for Ni/NiO_4(700 Å) and Ni/NiO_{50}(700 Å). (c) X-ray reflectivity scans for Ni/NiO_{25}(700 Å) (●) and Ni/NiO_{25}(220 Å) (○). (d) X-ray reflectivity scans for NiO_4(700 Å) and NiO_{50}(700 Å). Vertical lines (- - -) indicate the position of the critical wave vectors.

performed on all samples and for all P. Figure 2(b) shows the interplanar spacing evolution with P, obtained from the (111) NiO Bragg peaks in [Ni(53 Å)/NiO_P(700 Å)]. The reduction of P resulted in an enhancement of the uniform strain shown by the evolution of the interplanar spacings. Out of plane coherence lengths were obtained by inserting the observed values of full width at half maximum (FWHM) into the Scherrer equation. For all P, the out of plane coherence length was smaller than the crystallite height observed by TEM. In the absence of nonuniform strain, the coherence length would be equal to the crystallite height in our measurements.[28] This demonstrates that nonuniform strain is present and is increased when P is reduced. The limiting factor of the coherence length is the nonuniform strain induced by short range defects. For thin and thick NiO layers, the FWHM of the x-ray peaks for a given P is found to be the same, as shown in Fig. 3(a). This indicates that the defect concentration, revealed by nonuniform strain, is stable with thickness but is pressure dependent. It should be noted that identical measurements were obtained whether NiO was grown on Ni or glass. This demonstrates that the structural change induced by P was not confined at the interface but was an internal property of the NiO layer.

In addition to the crystalline ordering, we probed the evolution of the interfacial width and the density by taking x-ray reflectivity measurements. In these measurements, the intensity of the oscillations, named Kiessig fringes, depends on the electronic density profile of the structure.[28] Figure 3(b) shows the specular reflectivity data obtained for [Ni(53 Å)/NiO_4(700 Å)] and [Ni(53 Å)/NiO_{50}(700 Å)]. At the highest pressure, well defined Kiessig fringes arise from the Ni and NiO layers, indicating an abrupt interface and a low surface roughness. When P is decreased, the high frequency fringes arising from the NiO layer were attenuated, indicating changes in the electronic density, whereas the low frequency ones arising from the Ni layer were maintained. In these measurements, the critical wave vector depends on the electronic density of the top layers.[28] The critical wave vector changed from the Ni_1O_1 value (0.051 $Å^{-1}$) toward lower values when P was decreased, as shown in Fig. 3(b). The Ni volume fractions were obtained using the critical wave vector values.[29] The Ni volume fraction was 0.5, 0.46, 0.44, and 0.38 for $P(\times 10^{-3}$ mbar)=50, 25, 17, and 4 respectively. Ni_1O_1 was therefore obtained for $P=50\times 10^{-3}$ mbar. EDS was also used to probe the NiO stoichiometric changes induced by P. Figure 4 shows the [Ni(53 Å)/NiO_P(700 Å)] spectrum. When P decreases from 50×10^{-3} to 4×10^{-3} mbar, the integrated intensity of the 7.48 keV Ni peak decreases by 15%, as shown in the inset of Fig. 4. It reveals the decrease of the Ni concentration within the NiO layer and confirms the XRR measurements. Figure 3(c) shows that the critical wave vector does not depend on the NiO thickness. Thus, stoichiometric changes are not thickness dependent but pressure dependent. It should be noted that similar pressure effects were observed whether NiO was grown on Ni or glass, as shown in Fig. 3(d). Thus, structural changes induced by P do not depend on the interface but on the internal part of the NiO.

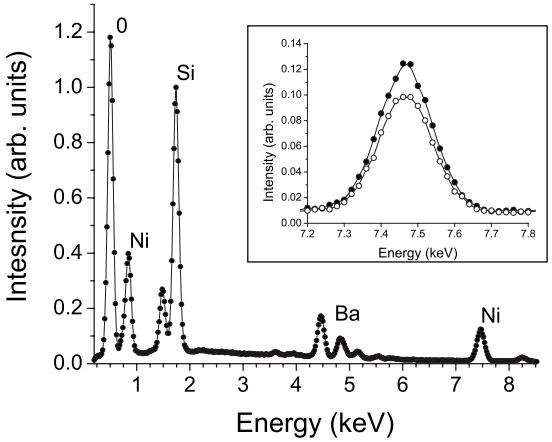

FIG. 4. Energy dispersive x-ray spectroscopy measurements for Ni/NiO_{50}(700 Å). Inset: Zoom on the Ni peak for Ni/NiO_{50}(700 Å) (●) and Ni/NiO_4(700 Å) (○).

To summarize, the evolution of the electronic density and uniform strain with the reduction of P shows an increase of the oxygen content in the NiO layer. Ni_1O_1 is obtained at the highest pressure. Stoichiometric changes induce an increased number of defects. These pressure dependent modifications are not thickness dependent. The $[Ni/NiO_P]$ magnetic properties are now studied to understand the driving mechanism of exchange anisotropy properties in such a system.

III. MAGNETIC PROPERTIES

Magnetization reversal loops were recorded simultaneously along the longitudinal and transverse directions using a vectorial vibrating sample magnetometer for all samples. We have also measured hysteresis loops at various α angles between the sample and the applied magnetic field. In the following, $\alpha=0$ when the applied field during VSM measurements is in the same direction as the applied magnetic field during growth. First, we present the Ni/NiO_P exchange and coercive field dependence on the NiO_P thickness. Following this, we examine the role of domains in the magnetization reversal using $Ni/NiO_{P_1}/NiO_{P_2}$ trilayers. P_1 and P_2 are two different argon pressures during growth. Finally, we study the angular dependence of the magnetic properties in order to characterize the asymmetry of the magnetization reversal.

A. H_e and H_c thickness dependence

When the applied field during VSM measurement is along the same direction as the applied field during growth, i.e., $\alpha=0$, the longitudinal hysteresis loop is symmetric and is shifted along the field axis when the NiO thickness is greater than a critical value. Furthermore, no magnetization is detected along the transverse direction, as shown in Fig. 5(b). The orientation of the net sample magnetization at the coercive and saturation fields was confirmed by PNR measurements. Polarized neutron reflectivity involves specular reflection of a polarized neutron beam onto a polarization analyzer.[30] Four neutron cross sections were measured. Two cross sections correspond to the non-spin-flip reflectivity profiles, where the intensities of reflected spin-up (↑↑) and spin-down (↓↓) neutrons illuminating and reflecting from the sample were measured. The difference between these two cross sections is related to the projection onto the direction of the applied field of the net sample magnetization averaged over the lateral dimensions of the sample. The remaining two cross sections are the spin-flip reflectivities, in which the incident neutron spin is changed after interaction with the sample magnetization. If the magnetization vector is perpendicular to the neutron spin, the neutron polarization will change and spin-flip scattering will be observed. The corresponding small spin-flip scattering in Figs. 5(a) and 5(c) indicates the negligible amount of transverse magnetization component at H_c and confirms the VSM measurements. Such observations rule out a coherent rotation reversal when the

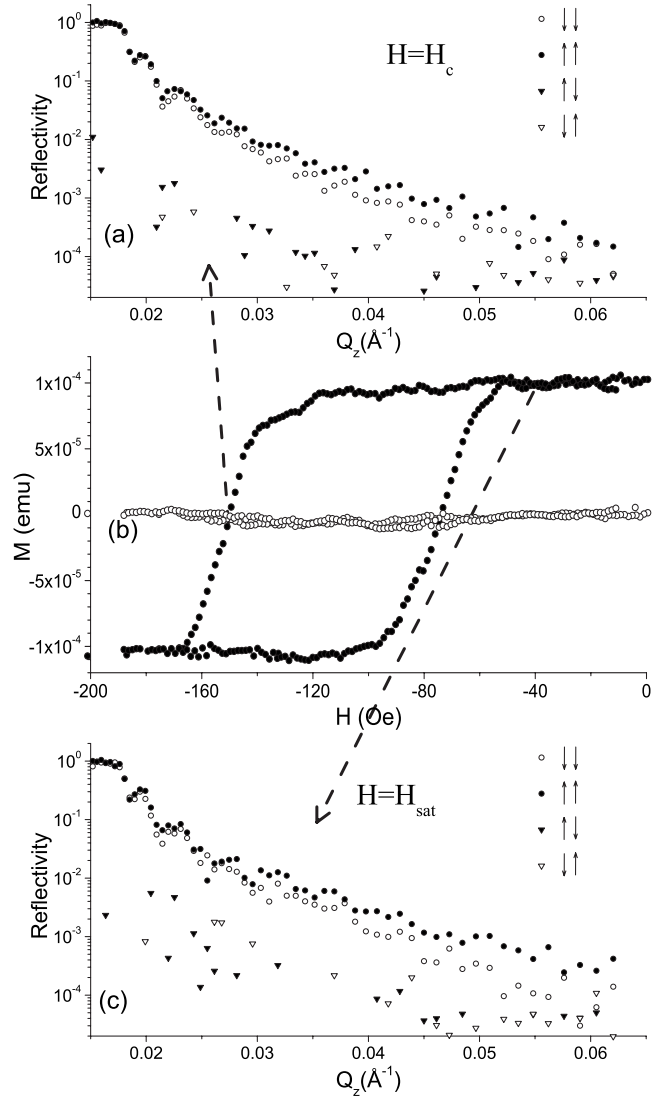

FIG. 5. (a) Four polarized neutron reflectivity cross sections at the coercive field. (b) Longitudinal (●) and transverse (○) magnetization loops. (c) Four polarized neutron reflectivity cross sections at saturation.

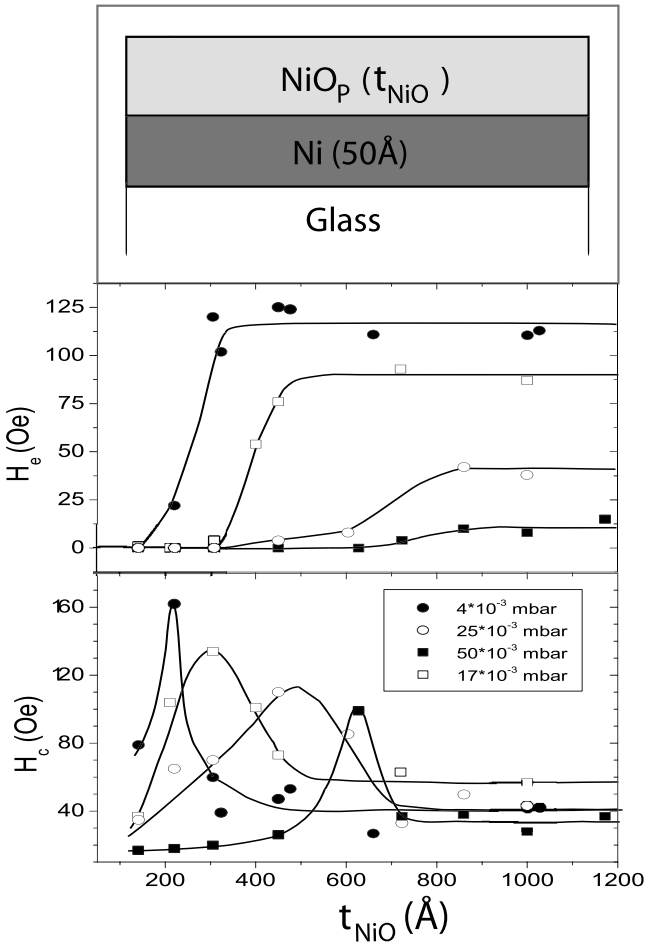

FIG. 6. H_c and H_e evolution with P and NiO thickness. The continuous lines are guides for the eye. Top panel: Scheme of the structure.

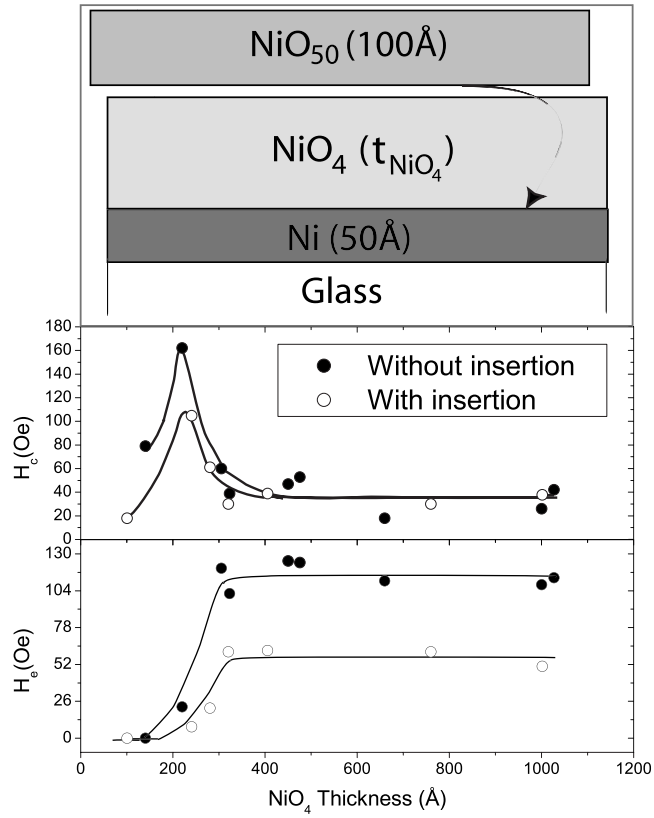

FIG. 7. H_e and H_c evolution with thickness in [Ni(53 Å)/NiO$_{50}$(100 Å)/NiO$_4$(t)]. Top panel: Scheme of the structure.

field is applied along the easy axis. The nucleation of DWs, perpendicular to the interface, must be taken into account to understand the exchange properties in our system. A planar-type DW could explain only locally the exchange anisotropy properties.

The influence of the NiO thickness and structural disorder on the unidirectional and coercive field is shown in Fig. 6. For all disorder states within the AF, the presence of a critical thickness t_c is shown. For such a thickness, H_e differs from zero to reach a saturated value and H_c is maximum. Within random-field-type models, H_e differs from zero when the AF anisotropy energy is sufficiently large as to hold nonreversible AF spins in place.[11] In models including the formation of a parallel DW at the interface, H_e differs from zero if the thickness is greater than the DW width.[6,31] Figure 6 shows that the disorder introduced within the AF results in an increase of H_e and in the H_c maximum. Such disorder effects on H_e and H_c are explained in domain-state-type models, where disorder induces a random field, and in a modified Mauri's model,[8] where disorder may induce local anisotropy enhancement. To understand the driving mechanism of the H_e and H_c evolution with the NiO thickness and disorder, one needs to distinguish between these two classes of models.

B. Insertion

We have probed the presence of a parallel DW by studying [Ni(53 Å)/NiO$_{50}$(100 Å)/NiO$_4$(t_{NiO_4})] trilayers as a function of t_{NiO_4}: the thickness of the NiO layer presenting the highest H_e. Figure 7 shows that the critical thickness is not modified by the insertion of the interfacial layer. However, H_e and the H_c maximum are reduced. If the parallel domain wall was responsible for the exchange anisotropy, H_e would be proportional to the energy contained in the domain wall, i.e., $\propto (AK_u)^{1/2}$, with A the exchange constant and K_u the AF uniaxial anisotropy constant. The critical thickness would be proportional to the domain wall width, i.e., $(A/K_u)^{1/2}$. A change in the AF exchange or anisotropy constant will result in a change of both properties: t_c and H_e. In the case of a bilayer AF structure, the energy of the domain wall will be contained in both layers with a respective contribution depending on the width of the wall.[32] The reduction of H_e after insertion would show that part of the DW is contained in the first layer. Consequently, t_c would vary. The stability of t_c with the important reduction of H_e shows that parallel DWs do not drive the exchange anisotropy.

It should be noted that H_e and the H_c maximum have reduced values when there is insertion but not as low as in [Ni/NiO$_{50}$]. This confirms that even though exchange anisotropy is an interface phenomenon, the bulk plays a significant role in our system. Even if the random field originates in

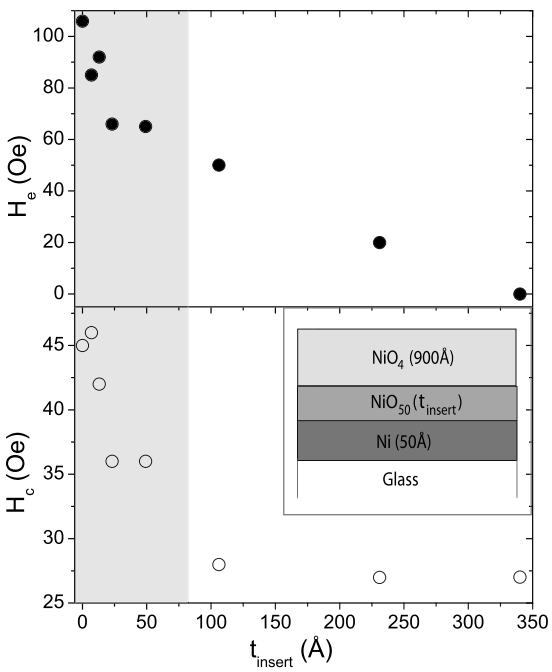

FIG. 8. H_e and H_c evolution with thickness in [Ni(53 Å)/NiO_{50}(t_{insert})/NiO_4(900 Å)]. The inset shows a scheme of the structure.

interfacial defects, domain walls have to propagate through the whole thickness.

To gain further information on the role of the bulk and the interface in the magnetization reversal, we have modified t_{insert}, the thickness of the NiO_{50} interfacial layer in [Ni(53 Å)/NiO_{50}(t_{insert})/NiO_4(900 Å)]. The NiO insertion results in reduced values of H_c and H_e, as shown in Fig. 8. H_c reaches a minimum equivalent to the bilayer [Ni(53 Å)/NiO_{50}(900 Å)] structure at $t_{insert} \approx 75$ Å. The strength of the Ni coercive field is modified by the overall AF structure and not only the interfacial properties. This coercive field depends on the AF anisotropy. Indeed, it requires weaker external fields to change the F spin direction which is coupled to a "smoother" AF spin.[11] Thus, the H_c reduced value due to the insertion reveals a weaker AF anisotropy due to the NiO_{50} insertion. It can be understood since Ni/NiO_{50} bilayers exhibit a lower value of the H_c maximum than Ni/NiO_4 bilayers. These results reveal the increase of the NiO anisotropy due to stoichiometric changes. Csiszar *et al.*[33] have recently shown the dependence of the CoO magnetic properties on the strain. In particular, the evolution of the CoO anisotropy was related to strain induced local crystal fields. In our study, the anisotropy is also modified by strain effects, suggesting a similar mechanism in NiO and CoO. Further experimental studies on NiO strained layers would be useful to conclude on such a point.

Figure 8 shows that H_e does not vanish after the insertion of a very thin NiO_{50} layer. It indicates that a coupling between the two AF layers is present. Indeed, if not coupled with NiO_4 spins, the NiO_{50} spins would be reversible at such a low thickness due to the Ni/NiO_{50} interfacial coupling. Thus, the exchange field would vanish if there was no coupling with the thick NiO_4 layer. The NiO_{50}/NiO_4 interface is responsible for the presence of nonreversible spins at the Ni/NiO_{50} interface. Considering the domain state model, the number of interfacial nonreversible spins depends on the domain state of the AF. In our study, DWs would have to propagate through NiO_{50} and NiO_4 layers. The NiO_4 layer affects the nonreversible spins at the Ni/NiO_{50} interface through its influence on the domain configuration of the whole structure. Such a long range effect could be used to tune exchange-bias properties.

Above 75 Å, i.e., outside the gray area in Fig. 8, H_e decreases whereas H_c is constant. It reveals that the driving mechanism leading to H_c is different from the one leading to H_e. The trilayer structure allows a variable H_e with constant saturation magnetization and constant H_c. It reveals the crucial role of the internal part of the AF and the need to include the AF multidomain structure to understand and control the unidirectional properties. In the following part, we present experimental evidence for the role of the AF multidomain structure for the Ni/NiO asymmetric magnetization reversal.

C. Angular dependence of magnetization reversal

The angular dependence of magnetization reversal provides information concerning axial and unidirectional anisotropic properties. We measured the net transverse magnetization component on both sides of the hysteresis loop at various angles. M_{up} (M_{down}) is the maximum of the transverse component for increasing (decreasing) field branches, as shown in Fig. 9(c). M_s is the saturation magnetization. Figure 9 shows the $|M_{up}/M_s|$ angular dependence in [Ni(53 Å)/NiO_4(t_{NiO})], where t_{NiO}, the thickness of the NiO layer exhibiting the greatest H_e, is set to 0, 120, and 1000 Å.

For a single Ni layer (t_{NiO}=0 Å), we observe an in-plane symmetry. It should be noted that such a symmetry is reproduced in the H_c angular dependences. This symmetry corresponds to the (111) threefold symmetry of fcc Ni and indicates a (111) texture of the Ni layer.

Adding a 120 Å NiO layer (i.e., thinner than the critical thickness), the symmetry is maintained. However, the magnetization reversal is modified as evidenced by the $|M_{up}/M_s|$ maximum value evolving from 25% when t_{NiO}=0 Å to 63% when t_{NiO}=120 Å. In F/AF systems, the H_c enhancement reveals modifications of the reversal. However, the observation of this enhancement is not sufficient to draw conclusion on the nature of these modifications. In our study, we show that such an enhancement may be related to different mechanisms of reversal.

Adding a NiO layer thicker than the critical thickness results in uniaxial and unidirectional anisotropy. In agreement with this uniaxial character, M_{up} is equal to M_s when the field is applied along the hard axis (α=90°), as shown in Fig. 9. It shows a coherent rotation reversal mechanism along the hard axis. These results reveal that the unidirectional and uniaxial anisotropic properties are induced by the NiO properties. The Ni reversal mechanism is driven by the NiO anisotropic properties and the domain configuration. Using x-ray photoemission electron microscopy, Blomqvist *et al.* have recently shown that unidirectional anisotropy

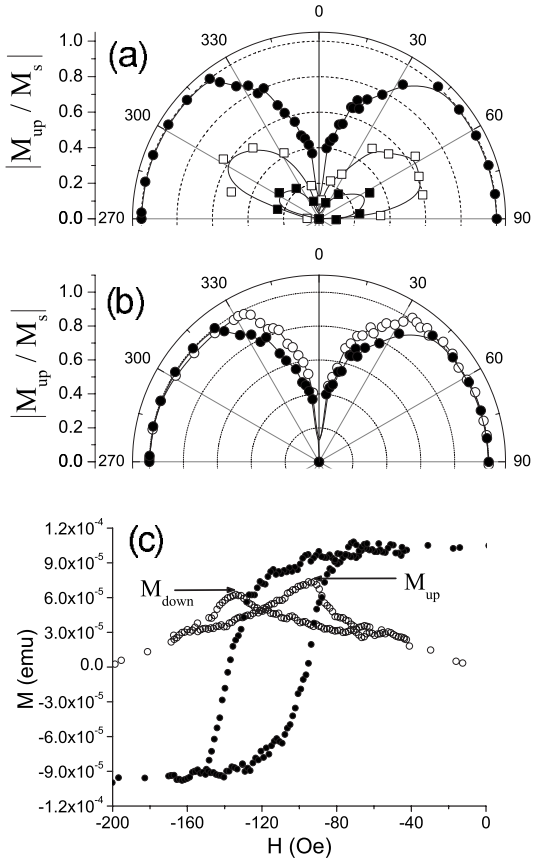

FIG. 9. (a) Angular dependence of $|M_{up}/M_s|$ of Ni/NiO$_4$(0 Å) (■), Ni/NiO$_4$(120 Å) (□), and Ni/NiO$_4$(1000 Å) (●). (b) Angular dependence of $|M_{up}/M_s|$ of Ni/NiO$_4$(1000 Å) (●) and Ni/NiO$_4$(1000 Å) (○). (c) Longitudinal and transverse loops of Ni/NiO$_4$(1000 Å) at α=14°.

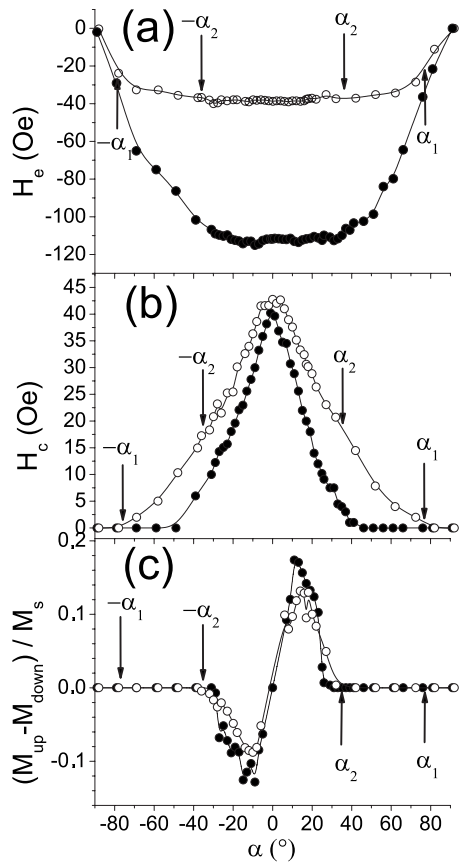

FIG. 10. Angular dependence of (a) H_e, (b) H_c, (c) normalized M_{up}, and (d) asymmetry of [Ni(53 Å)/NiO$_4$(1000 Å)] (filled circle) and [Ni(53 Å)/NiO$_{25}$(1000 Å)] (open circle). For clarity, critical angles, α_1 and α_2, are only drawn for the [Ni(53 Å)/NiO$_{25}$(1000 Å)] sample.

strongly affects the overall magnetic domain structure and leads to the asymmetric magnetization reversal.[34] Our study reveals a similar mechanism in Ni/NiO and brings evidence for a modification of the overall reversal mechanism, and not only a modification of H_c, that occurs before the appearance of H_e. In the following, we study the asymmetry of the magnetization reversal to understand its dependence on coherent rotation and domain nucleation.

The contributions of coherent rotation and domain nucleation to the asymmetry and its angular dependence are outlined but their respective role is still unclear. Recent studies have shown that features of the angular dependence of the asymmetry can be reproduced by coherent rotation reversal.[23,25] We have probed the angular dependence of the asymmetry in our system in order to study the effect of noncoherent reversal. We quantify the asymmetry as $(M_{up}-M_{down})/M_s$, where M_{up} (M_{down}) is the maximum of the transverse component for increasing (decreasing) field branches, and M_s is the saturation magnetization.

The angular dependence of [Ni(53 Å)/NiO$_4$(1000 Å)] and of [Ni(53 Å)/NiO$_{25}$(1000 Å)] exhibit a first critical angle, α_1, corresponding to the onset of coercivity, as shown in Fig. 10. At this angle, M_{up} is equal to the saturation magnetization M_s and the asymmetry is zero. The reversal is then a coherent rotation. Using the Stoner and Wohlfarth model, α_1 is defined as $\arctan(2K_u/K_e)$, where K_u is the uniaxial anisotropy constant determined from the hard axis loop and K_e $(=H_eM_s)$ is the unidirectional anisotropy constant.[23] The predicted α_1 value is 72° (47°) in [Ni(53 Å)/NiO$_{25}$(1000 Å)] ([Ni(53 Å)/NiO$_4$(1000 Å)]) and is in very good agreement with the observed experimental value. However, the onset of asymmetry occurs at a second critical angle, α_2, corresponding to the decrease of (M_{up}/M_s). At this critical angle, nonuniform reversal, i.e., a multidomain structure, is shown by such a decrease. Our results are different from those obtained using the Stoner and Wohlfarth model. In their model, the critical angle is at the onset of the coercivity and asymmetry ($\alpha_1=\alpha_2$). However, in our study, the coercivity vanishes after the asymmetry ($\alpha_1 > \alpha_2$). The coherent rotation mechanism fails to describe the features of our system and nonuniform reversal should be considered. Numerical simulations based on the domain state model have recently predicted that the nonuniform reversal mode leads to the asymmetry and its angular dependence.[26] Our experimental study supports such a prediction and outlines the relevance of domain formation in the asymmetry.

The asymmetry of the magnetization reversal is found to be greater when the ratio K_u/K_e decreases. It reveals a rich behavior and further studies would be useful to predict and/or measure a second critical angle in other systems.

IV. CONCLUSION

In this Ni/NiO experimental study, we have modified the NiO microstructure by changing the stoichiometry through the control of argon pressure during the sputtering growth. Nonstoichiometric NiO contains more defects resulting in a decrease of the coherence length in XRD measurements. A systematic study of H_e and H_c as a function of NiO thickness reveals the enhancement of H_e and of the H_c maximum value with nonstoichiometric NiO. Such a phenomenon is predicted by models including parallel and perpendicular domain walls. We show that parallel domain walls do not drive this enhancement since inserting a different NiO layer at the interface does not change the critical thickness. In models including AF perpendicular DWs, the exchange properties (H_e, H_c, and t_c) depend on the AF domain state driven by the AF microstructure. Our Ni/NiO structures exhibit such a dependence and support the domain state model.

We show that H_c and H_e are not directly related in the sense that one can change one of them without changing the other one. It reveals the crucial role of the internal part of the AF. We show that Ni unidirectional and uniaxial properties originate from the Ni/NiO interfacial coupling. It reveals the need to include the AF multidomain structure to understand and control the axial and unidirectional properties in Ni/NiO. In our system, the angular dependence of the exchange properties is not explained by the Stoner and Wohlfarth model as it exhibits two critical angles. The first angle corresponds to the onset of coercivity and the second corresponds to the onset of nonuniform reversal and asymmetry. The multidomain structure should be included in the reversal mechanism to understand the asymmetry of the magnetization reversal and exchange properties in the studied polycrystalline Ni/NiO structures.

ACKNOWLEDGMENTS

We acknowledge the Rutherford Appleton Laboratory for the provision of neutrons.

*david.dekadjevi@univ-brest.fr

[1] W. H. Meiklejohn and C. P. Bean, Phys. Rev. **102**, 1413 (1956).
[2] W. H. Meiklejohn and C. P. Bean, Phys. Rev. **105**, 904 (1957).
[3] J. Nogues and I. K. Schuller, J. Magn. Magn. Mater. **192**, 203 (1999).
[4] A. E. Berkowitz and K. Takano, J. Magn. Magn. Mater. **200**, 552 (1999).
[5] C. H. Marrows, S. Langridge, M. Ali, A. T. Hindmarch, D. T. Dekadjevi, S. Foster, and B. J. Hickey, Phys. Rev. B **66**, 024437 (2002).
[6] D. Mauri, H. C. Siegmann, P. S. Bagus, and E. Kay, J. Appl. Phys. **62**, 3047 (1987).
[7] P. Steadman, M. Ali, A. T. Hindmarch, C. H. Marrows, B. J. Hickey, S. Langridge, R. M. Dalgliesh, and S. Foster, Phys. Rev. Lett. **89**, 077201 (2002).
[8] J. V. Kim and R. L. Stamps, Phys. Rev. B **71**, 094405 (2005).
[9] A. P. Malozemoff, Phys. Rev. B **35**, 3679 (1987).
[10] U. Nowak, K. D. Usadel, J. Keller, P. Miltenyi, B. Beschoten, and G. Guntherodt, Phys. Rev. B **66**, 014430 (2002).
[11] A. Misra, U. Nowak, and K. D. Usadel, J. Appl. Phys. **95**, 1357 (2004).
[12] Z. Li and S. Zhang, Phys. Rev. B **61**, R14897 (2000).
[13] R. Shan, W. W. Lin, L. F. Yin, C. S. Tian, H. Sang, L. Sun, and S. M. Zhou, Phys. Rev. B **71**, 064402 (2005).
[14] C. Leighton, M. R. Fitzsimmons, A. Hoffmann, J. Dura, C. F. Majkrzak, M. S. Lund, and I. K. Schuller, Phys. Rev. B **65**, 064403 (2002).
[15] L. Wang, B. You, S. J. Yuan, J. Du, W. Q. Zou, A. Hu, and S. M. Zhou, Phys. Rev. B **66**, 184411 (2002).
[16] C. Leighton, J. Nogues, B. J. Josson-Akerman, and I. K. Schuller, Phys. Rev. Lett. **84**, 003466 (2000).
[17] Z. Qian, J. M. Sivertsen, and J. H. Judy, J. Appl. Phys. **83**, 6825 (1998).
[18] M. R. Fitzsimmons, P. Yashar, C. Leighton, I. K. Schuller, J. Nogues, C. F. Majkrzak, and J. A. Dura, Phys. Rev. Lett. **84**, 3986 (2000).
[19] P. Gogol, J. N. Chapman, M. F. Gillies, and C. P. Bean, J. Appl. Phys. **92**, 1458 (2002).
[20] E. Pina, C. Prados, and A. Hernando, Phys. Rev. B **69**, 052402 (2004).
[21] F. Radu, A. Westphalen, K. Theis-Brohl, and H. Zabel, J. Phys.: Condens. Matter **18**, L29 (2006).
[22] T. Mewes, H. Nembach, M. Rickart, S. O. Demokritov, J. Fassbender, and B. Hillebrands, Phys. Rev. B **65**, 224423 (2002).
[23] J. Camarero, J. Sort, A. Hoffmann, J. M. Garcia-Martin, B. Dieny, R. Miranda, and J. Nogues, Phys. Rev. Lett. **95**, 057204 (2005).
[24] L. Spinu, A. Stancu, Y. Kubota, G. Ju, and D. Weller, Phys. Rev. B **68**, 220401(R) (2003).
[25] A. Tillmanns, S. Oertker, B. Beschoten, G. Guntherodtand, J. Eisenmenger, and I. K. Schuller, arXiv:cond-mat/0509419v2 (unpublished).
[26] B. Beckmann, U. Nowak, and K. D. Usadel, Phys. Rev. Lett. **91**, 187201 (2003).
[27] D. T. Dekadjevi, A. Suvorova, S. Pogossian, D. Spenato, and J. B. Youssef, Phys. Rev. B **74**, 100402(R) (2006).
[28] P. F. Fewster, Rep. Prog. Phys. **59**, 1339 (1996).
[29] P. F. Miceli, D. A. Neumann, and H. Zabel, Appl. Phys. Lett. **48**, 24 (1986).
[30] G. P. Felcher, R. O. Hilleke, R. K. Crawford, J. Hanmann, R. Kleb, and G. Ostrowski, Rev. Sci. Instrum. **58**, 609 (1987).
[31] H. Xi and R. M. White, Phys. Rev. B **61**, 80 (2000).

[32] H. Kronmuller and M. Fahnle, *Micromagnetism and the Microstructure of Ferromagnetic Solids* (Cambridge University Press, Cambridge, UK, 2003).

[33] S. I. Csiszar, M. W. Haverkort, Z. Hu, A. Tanaka, H. H. Hsieh, H.-J. Lin, C. T. Chen, T. Hibma, and L. H. Tjeng, Phys. Rev. Lett. **95**, 187205 (2005).

[34] P. Blomqvist, K. M. Krishnan, and H. Ohldag, Phys. Rev. Lett. **94**, 107203 (2005).